JEAS

JOURNAL OF ENGINEERING AND APPLIED SCIENCES

Journal of Engineering and Applied Sciences, Volume 21, Number 1, Dec. 2022, 876 - 885

Influence of Magnetic Properties on the Performance of Dual Stator Electric Machine: Part II

Chukwuemeka C. Awah[1*]
[1]Department of Electrical and Electronic Engineering, Michael Okpara University of Agriculture, Umudike, Nigeria
[*]Corresponding Author's E-mail: awahchukwuemeka@gmail.com

Abstract
Magnetic properties such as magnet coercive force and magnetic remanence have significant impact on the electromagnetic performance of an electric machine. Thus, detailed analysis on the characteristics of these magnetic properties for better understanding of precise magnet material selection is demonstrated in this work. The investigated machine features include: torque-speed profile, total harmonic distortion (THD), torque ripple and winding inductances. Maxwell-2D finite element software is used in the analysis. It is shown that the investigated machine type having neodymium magnet has the most admirable qualities such as larger output torque, higher saturation-withstand potential than others, etc. Moreover, it is observed that the investigated machine output torque is more or less generated by its magnetic torque component with insignificant contribution made from the reluctance torque constituent. More so, the results reveal that there is an inverse relationship between the coercive forces of a given electric machine and its resulting winding inductance magnitudes. The estimated maximum quadrature-axis inductance of the investigated machine is: 0.6275 mH, 0.5567 mH, 0.3760 mH and 0.2873 mH i.e. from alnico, ferrite, SmCo and NdFeB magnets, respectively, with the following corresponding coercive force: 230 kA/m, 303 kA/m, 796 kA/m and 1063 kA/m, respectively. Above all, electrical machine designers could through this analysis have better understanding on the right choice of magnetic material, which invariably depends on specific application.

Keywords: Copper loss, Current, Dual stator, Magnetic properties and Winding inductances.

1. Introduction

In order to lessen the global energy crisis, more research attention is currently being made towards electromagnetic and energy conversion devices with low energy product profiles; however, with improved environmental-friendly features. Therefore, magnet coercive force and magnetic remanence amplitudes, which constitute the key magnetic properties of a magnet, are important performance criteria used in determining the output of a given electrical machine/device and its consequential effects. Hence, the magnetic properties of four (4) different kinds of magnets i.e. ferrite, alnico, neodymium (NdFeB) and samarium-cobalt (SmCo) are quantitatively compared and presented in this study for better understanding of proper material usage for any given machine application (s). The ferrite and alnico are categorized as non-rare-earth magnets while NdFeB and SmCo are classified as rare-earth magnets. The rare-earth magnets usually have both higher coercive force (coercivity) and larger magnetic remanence than its non-rare-earth counterparts.

Ghorbanian et al, (2018) proved that material properties of both the core sections and magnet areas of electrical machines are indispensable in the machines' output performance, coupled with the materials' temperature tolerances which also rely on other operating conditions/modes of the machines. Meanwhile, Soleimani et al, (2014) showed that increased temperature effect would have depreciating consequence on both the magnetic coercivity and remanence flux density of the machine, particularly at high operating temperature and eventually would result to lower output performance of the machine. Deplorably, the NdFeB magnet has high vulnerability to temperature effect compared to other magnet materials, despite its enviable electromagnetic performance. The impact of material selection on the output performance of a machine is re-emphasized in Husain et al, (2018).

The use of alnico magnets on electric machines would naturally boost its speed range and also enhance the machine's fault-tolerance skill, besides its cost-effectiveness compared to the rare-earth magnetic electric machines, as proved in Zhu et al, (2015). These qualities are possible due to the intrinsic flux-regulation flexibility of the alnico magnetic material. It is worth noting that despite the high remanence flux density of alnico materials, it still exhibit low energy product profile, owing to its poor coercive force, and this demerit will eventually lead to its drastic inferior electromagnetic performance, as noted in Zhu et al, (2016). More so, Husain et al, (2018) established that a ferrite magnet could be used to achieve a reasonable torque density and power from a given electric machine, if magnetic field-converging technique is applied to the magnets through its placement plan and orientation; thereby, improving the overall airgap flux density for enhanced performance. Additionally, proper optimization of the leading design elements would also help to positively advance the electromagnetic output of a machine.

Nevertheless, a more economical design of electrical machine would be realized through integration of rare-earth and non-rare-earth magnets in one electrical system in the ratio of 3:2, in order to reduce the high cost of rare-earth magnet through proper reduction of its volume usage, without sacrificing substantial amount of its electromagnetic yield. This cost-saving design of integrating two different classes of magnet is demonstrated to be very effective and efficient in Chen et al, (2020). The importance of magnet integration of both rare-earth and non-rare-earth magnets is also strongly recommended in Wu et al, (2018), primarily for low cost gain.

The studies presented in Xia et al, (2014) reveal that tremendous performance could be realized from a given permanent magnet machine by replacing a rare-earth magnet with its non-rare-earth equivalent, using both flux-concentrating technique and increased winding layers of the machine. The studies also established that a non-rare-earth electric machine having double-layer winding pattern would match the performance of its rare-earth counterpart, even with reduced loss profile and lower torque ripple. Nevertheless, a single-layer flux-switching permanent magnet machine would produce the largest torque compared to other winding layers (Hwang, et al, 2014); albeit, with higher saturation weakness, despite its great fault-tolerance potential.

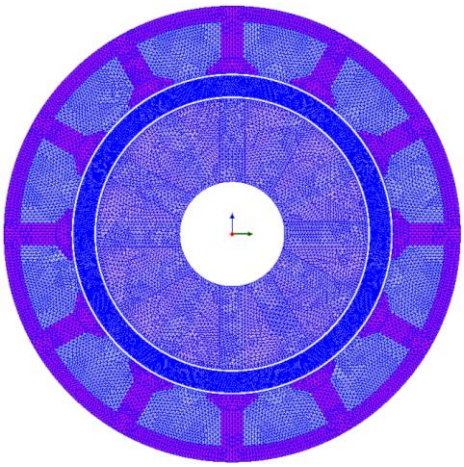

Figure 1: Two-dimensional mesh diagram

Further, it is highlighted in Yu et al, (2015) that non-rare-earth magnets particularly the alnico type, could provide an extended speed range for a given motor drive system; however, it is susceptible to irreversible demagnetization coupled with a low coercivity value, which would customarily affect the output performance of the machine, despite its high magnetic remanence worth. Similarly, an electric machine made with alnico magnets has high capability for torque ripple reduction and improved power factor, in addition to excellent reduced-cost quality, as proved in Maroufian and Pillay (2019).

In principle, the influence of magnetic material on the electromagnetic performance of dual stator flux-switching permanent magnet machine is investigated in this study using finite element approach; in order to provide better insight for electric machine designers on magnetic material selection. The original structural model of Figure 1 which represents the investigated machine is proposed in (Evans and Zhu, 2015).

2.0 Material and methods

2D-finite element analysis procedure is adopted in the prediction of the results in this study, with the aid of Maxwell-2D version 15 simulation software. A desktop computer with the following specifications is used in simulating the studied model: Intel (R) core i7, 3.40 GHz, an 8.00 GB RAM size and x64-based processor. TRANSIENT SOLVER of the software is adopted in the calculations due to its intrinsic ability to predict both time-varying electric and magnetic fields of a given machine model. The software user-friendly windows engaged in this work are: the menu bar, project manager, message messenger, property and progress windows. In the respective windows, both the dimensions of the model and its material properties are defined and assigned to the relevant parts from the in-built materials of the software. Two basic categories of the used magnets are: 1. Rare-earth magnets which comprise the neodymium (NdFeB) and samarium-cobalt (SmCo) magnetic materials. 2. Non-rare-earth magnets which are the ferrite and aluminum-nickel-cobalt (alnico) magnetic materials. The magnetic remanance of the compared machine types having ferrite, alnico, SmCo and NdFeB magnetic materials is 0.4 T, 1.16 T, 1.05 T, and 1.47 T, respectively. The employed magnets also have corresponding magnet recoil permeability of 1.05, 4, 1.05 and 1.1, respectively. More so, the compared machine has an active axial length of 25 mm and machine total radius of 45 mm. The size of its airgap is 0.5 mm. Note that the investigated machine has a modulating ring as a rotor, placed in-between its inner and outer stator sectors. Note also that the core materials are made of silicon steel materials, though better machine performance could be achieved, if the steel is replaced with cheaper and lower loss-content soft magnetic material; nevertheless, with fragile mechanical strength, as pointed out in Liu et al, (2017). The rated speed and current of the investigated machine is 400 rev/min and 15 Amperes, respectively. The supplied three-phase current in the compared machine is given in (1a)–(1c).

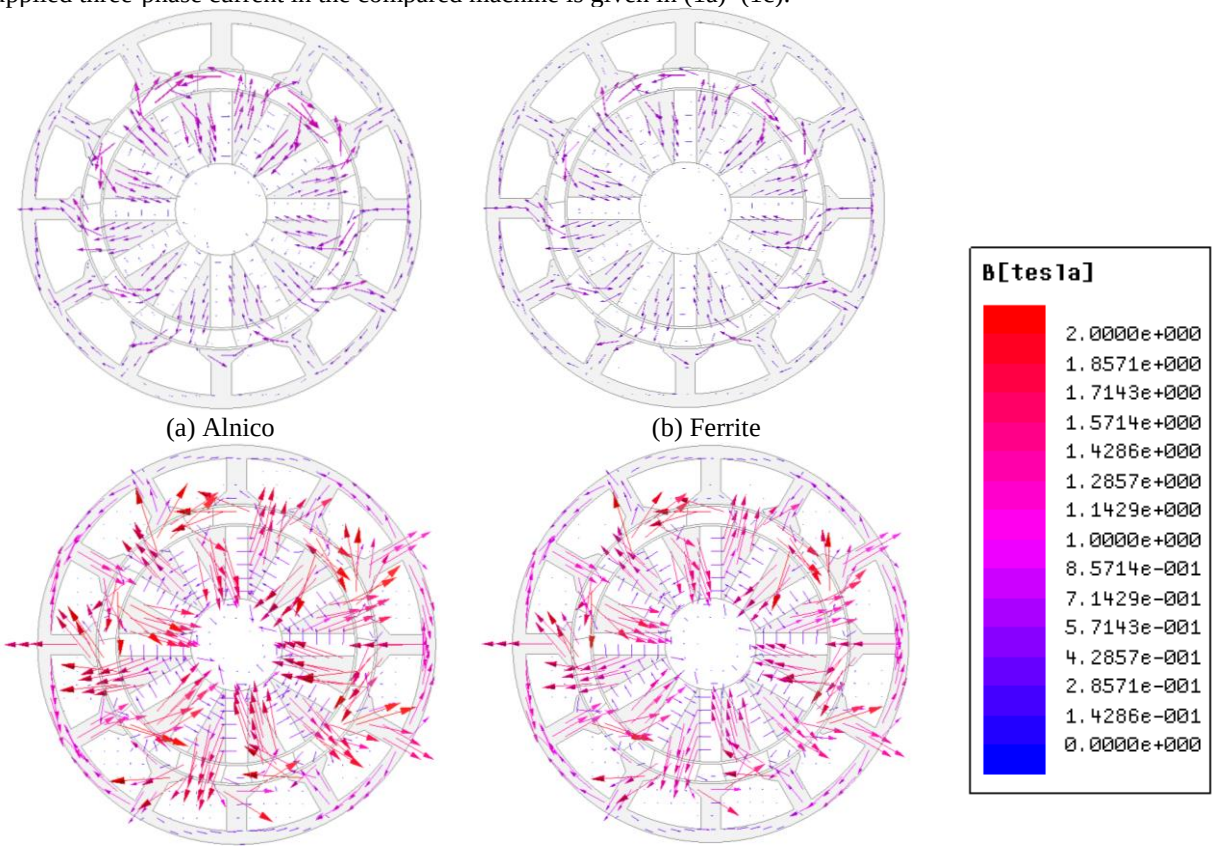

(a) Alnico (b) Ferrite

(c) NdFeB (d) SmCo

Figure 2: Magnetic field vector contours on no-load

$$I_A = I_{peak} \sin\theta \quad (1a)$$

$$I_B = I_{peak} \sin\left(\theta + \left(\frac{2\pi}{3}\right)\right) \quad (1b)$$

$$I_C = I_{peak} \sin\left(\theta + \left(\frac{4\pi}{3}\right)\right) \quad (1c)$$

where: I_A, I_B and I_C are the supplied phase currents, I_{peak} is the applied peak current value.

Figure 1 shows mesh plots of the investigated machine; the adopted tiny mesh elements would help to enhance the accuracy of the employed finite element method; however, it would involve longer simulation time. Moreover, magnetic field vector contours of the investigated machine are illustrated in Figure 2. It is worth noting that rare-earth magnetic machines have higher magnetic field vector concentration than its non-rare-earth counterparts.
Also, the predicted output torque, T_o, relation with winding inductances is expressed in equation 2.

$$T_o = \frac{N_{ph}}{2} P_r \left(\left(\Psi_m I_q \right) + \left(L_d - L_q \right) I_d I_q \right) \tag{2}$$

where: N_{ph} is the phase number, P_r is the number of rotor poles, L_d, L_q, are the direct-and quadrature-axis inductances, Ψ_m is the magnet flux, I_d, I_q are the matching axis currents (Chen et al, 2008).

3.0 Results and Discussions

The plotted graphs in this section emanated from the automatically computer-generated numerical data from the software, and these figures characterize the finite element predicted electromagnetic output of the compared models. Figure 3 show the waveforms of the analyzed machine's airgap coercive force and its resultant flux density magnitude in one electric revolution. The electromagnetic performance of a given permanent magnet machine is a function of its coercive force and airgap flux density values. It is observed that neodymium and SmCo magnetic machines have larger amplitudes of these parameters; hence, the most likely reason for their higher performance compared to ferrite and alnico magnetic machines. Maximum coercive force amount of about 1265.2458kA/m with a corresponding flux density of 1.5899 Tesla is recorded in the neodymium magnetic machine at the machine's airgap; while the least amount of airgap coercive force of approximately 449.3618 kA/m with resulting airgap flux density of 0.5647 Tesla is obtained in the ferrite-made machine.

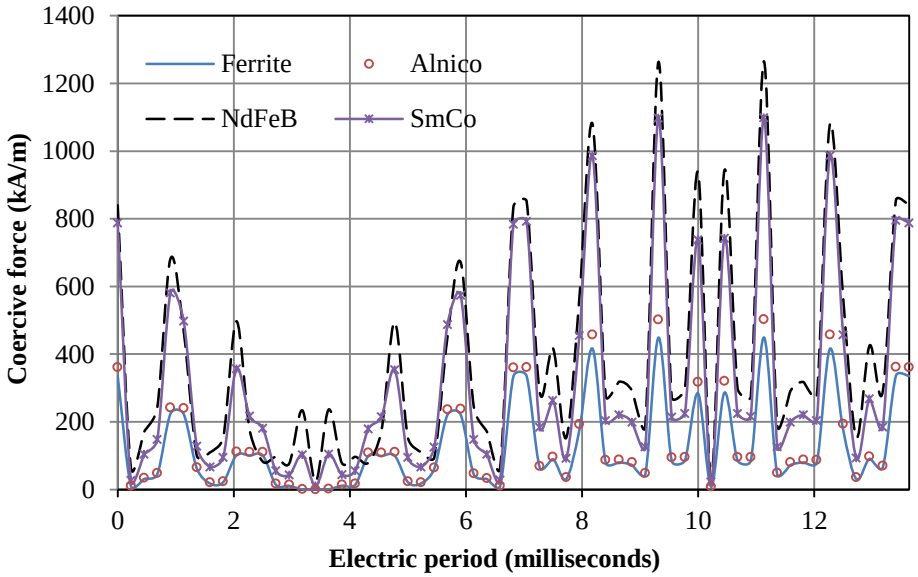

(a) Coercive force versus time

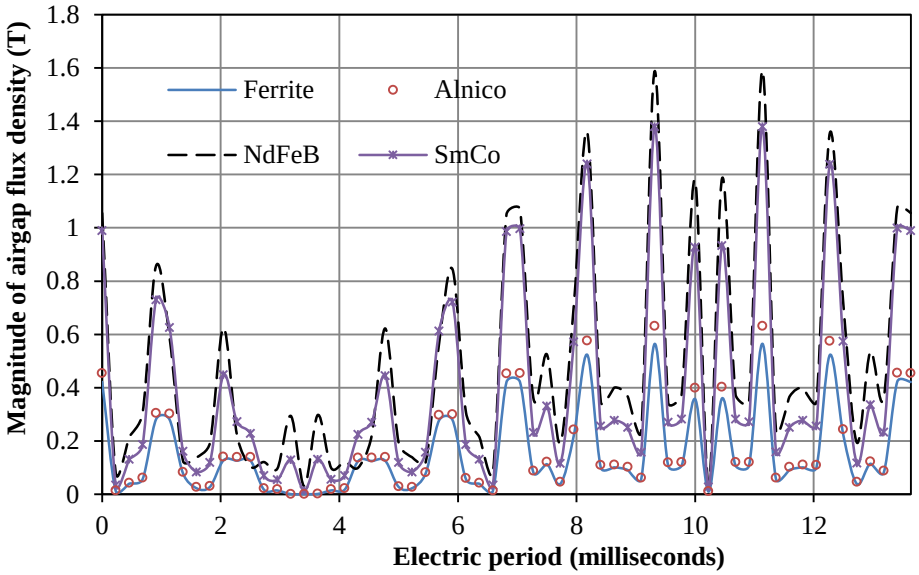

(b) Airgap flux density versus time

Figure 3: Comparison of magnetic coercive force and airgap flux density

Further, torque-speed envelope of the compared machine having different magnets is shown in Figure 4. It is revealed that the non-rare-earth magnetic machines would have larger speed coverage than its rare-earth equivalents; albeit, with lower output torque and by such, the non-rare-earth magnetic machines exhibit better flux-weakening potential i.e. in the constant power region of operation. The obtained maximum torque from the compared machines is: 1.31 Nm, 1.41 Nm, 3.00 Nm and 3.23 Nm for the machine having ferrite, alnico, SmCo and NdFeB, respectively. The predicted torque-speed curve is simulated with current amplitude of 15 Amperes and an inverter rated voltage of 22.9 Volts. Moreover, the predicted results show that large chunk of the generated torque of the analyzed machine is obtained from the magnetic component of torque with negligible amount being contributed from its reluctance part. Therefore, the machine would have nearly equal magnitudes of winding inductances in both the direct and quadrature axes of the machine (Chen *et al*, 2008). This assertion is illustrated in Figure 5, as seen from the almost similar amount of axes inductance. It is important to note that the investigated machine belongs to flux-switching permanent magnet machine class of electric machines. Moreover, it has equal winding inductances i.e. in the direct and quadrature axis. In as much as these equal inductance characteristics is appropriate for the analyzed machine category, owing to its inherent flux-switching phenomenon; however, it is preferable to have large difference between the axis inductances in most conventional permanent magnet machines, due to its saliency nature/relevance caused by its reluctance torque characteristics. It is worth mentioning that when the winding inductance in both axes has large discrepancy amongst its set of values; then, there would be higher tendency for such machines to withstand electric overload, especially at constant power region of operation, apart from the improved saliency ratio which will enhance the output of the machines considerably. This overload concept is highlighted in Wu *et al*, (2018).

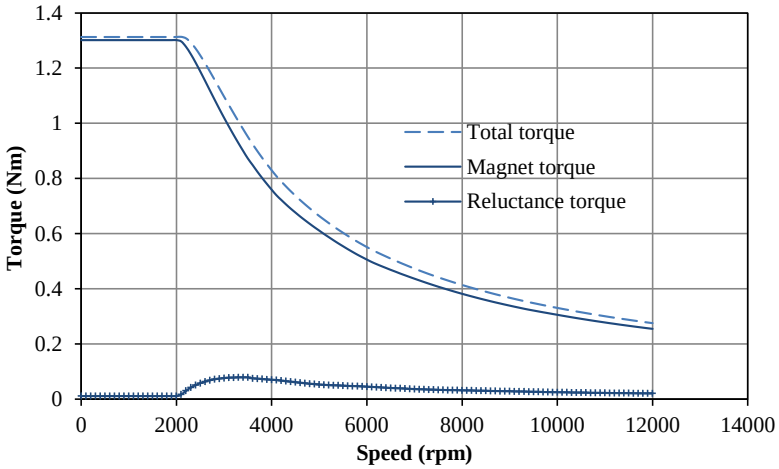

(a) Ferrite

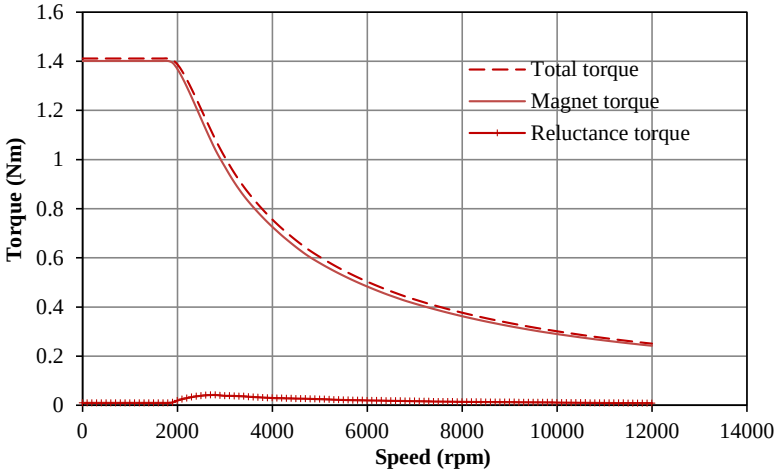

(b) Alnico

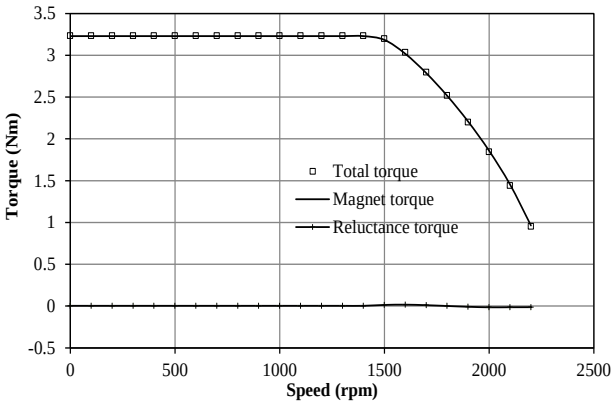

(c) NdFeB

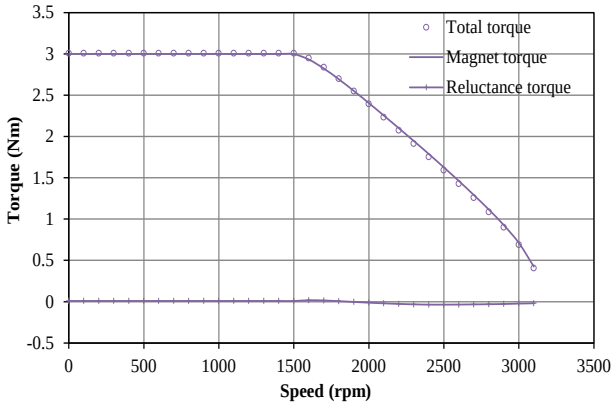

(d) SmCo

Figure 4: Comparison of torque at 15Amperes and 22.9Volts

Figure 5 shows the winding inductance waveforms of the simulated machine model over rotor angular positions, in one electric period. The plots show that winding inductances varies inversely proportional to the machine's coercive force or coercivity value. The obtained maximum quadrature-axis inductance of the machine is: 0.6275 mH, 0.5567 mH, 0.3760 mH, and 0.2873 mH, for alnico, ferrite, SmCo and NdFeB magnetic machines, respectively. Although, the inductance waveforms are uniformly distributed over the simulation period; the magnitude of these inductances would also slightly depend upon the rotor angular positions. More so, the magnitude of winding

inductances is correlated with its saturation withstand flaw. If the winding inductance of a given machine is high, then it will have lower ability to withstand saturation effect, and vice-versa. Therefore, the non-rare-earth magnetic machines would have weaker capability to withstand saturation effect than the rare-earth ones.

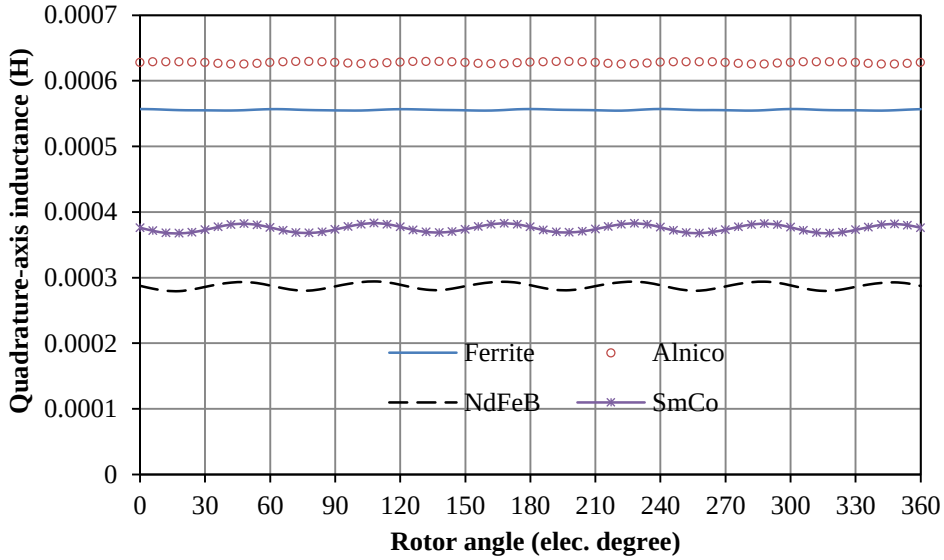

(a) Quadrature-axis inductance versus rotor angle

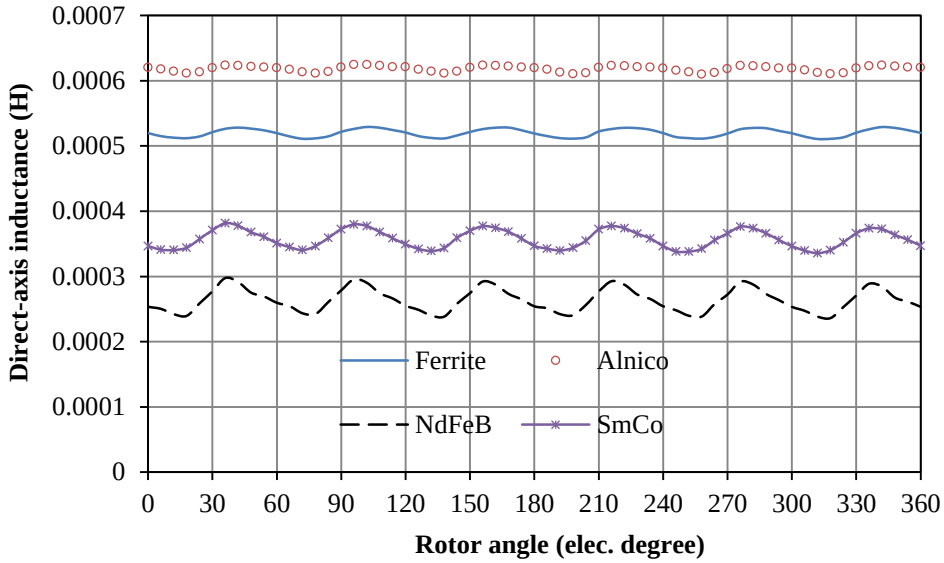

(b) Direct-axis inductance versus rotor angle

Figure 5: Comparison of axes inductance at quadrature current of 15Amperes

Furthermore, the generated fluxes in both direct and quadrature axis directions of the machine is depicted in Figure 6. It could be inferred that the quadrature-axis flux varies directly proportional to the applied quadrature-axis current, as seen in Figure 6(a). Similarly, the variation of direct-axis flux with current indicates that there is low sensitivity response of direct-axis flux to the applied quadrature-axis current, as seen in Figure 6(b). However, there would be a minor reduction in the direct-axis flux amplitude as the machine undergoes heavy electric loading, owing to the effect of armature reaction of phase windings. Meanwhile, the direct-axis flux values are higher in the rare-earth magnetic machines, since it constitute part of torque production mechanism of the simulated machine.

Figure 7 shows the comparison of total harmonic distortion (THD) plots of the induced voltage as well as torque ripple outlines of the analyze machine types, under different copper loss ratings. It is observed that the non-rare-

earth magnetic machines have higher total harmonic distortion as well as larger amount of torque ripple compared to its rare-earth equivalents. It is worth mentioning that these two indices i.e. THD and torque ripple are undesirable machine characteristics, since it has negative influence such as high cogging torque implication, increased noise and vibration in an electrical machine/device, in addition to inefficient control operation of the machine, etc. It is also inferred that the larger the copper loss amplitude in the machine, then, the higher its THD value. However, an inverse condition is almost obtainable in the variation of torque ripple with copper loss. Normally, the induced voltage of any given electrical machine is estimated on no-load condition; however, it is proved in Paula *et al*, (2018) that induced voltage of a machine on load is usually affected by the electromagnetic saturation effect of the windings; more so, the resulting impact of THD due to the induced load voltage would conversely affect the torque ripple outline of the device. Thus, an indirect relationship exists between the induced load voltage and its subsequent torque ripple formation.

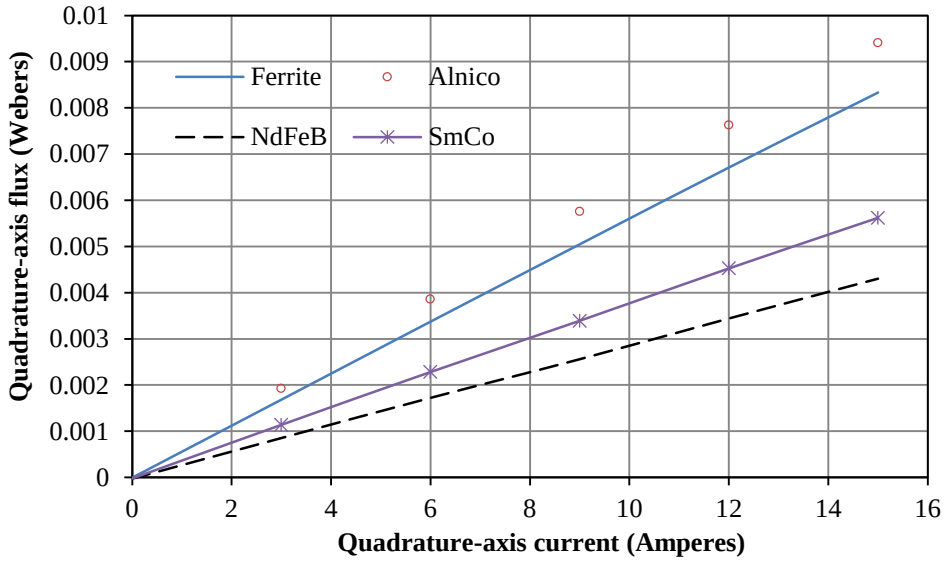

(a) Quadrature-axis flux versus quadrature-axis current

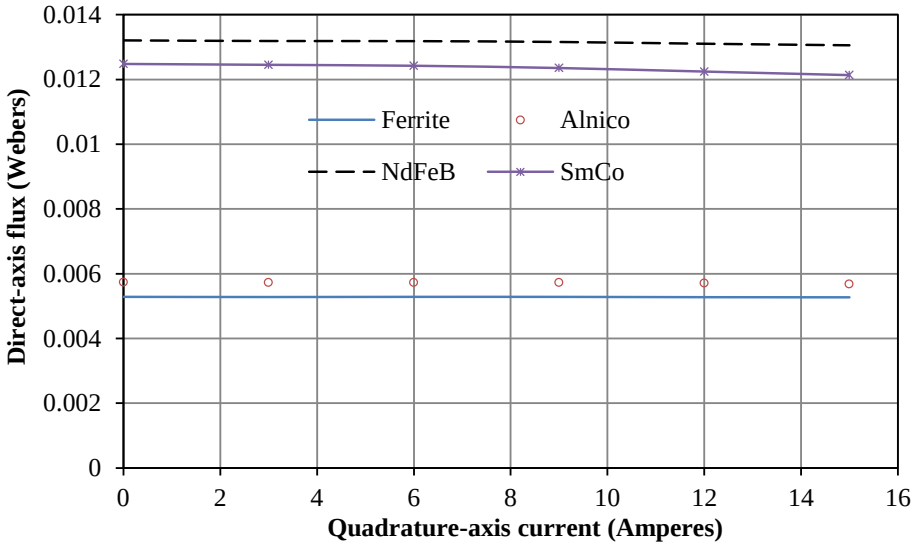

(b) Direct-axis flux versus quadrature-axis current

Figure 6: Comparison of axes flux at 400rpm

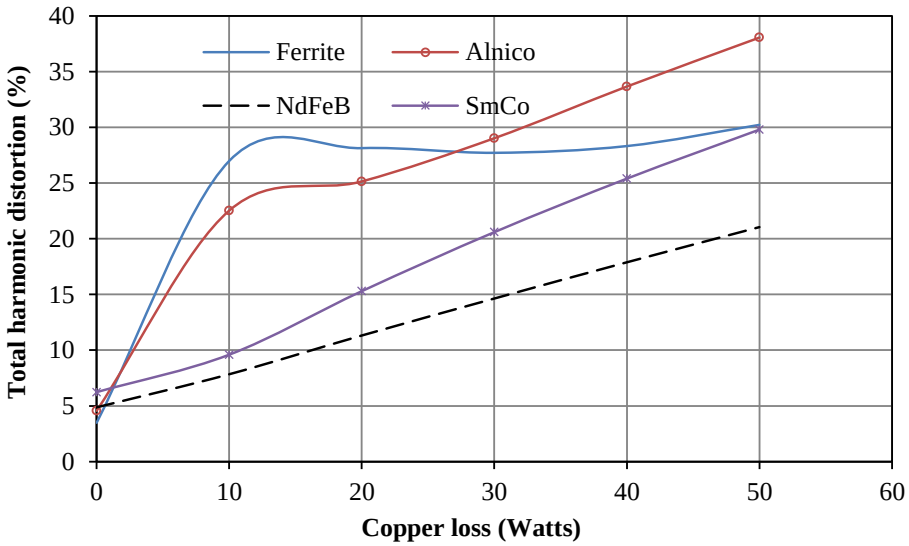

(a) Total harmonic distortion versus copper loss

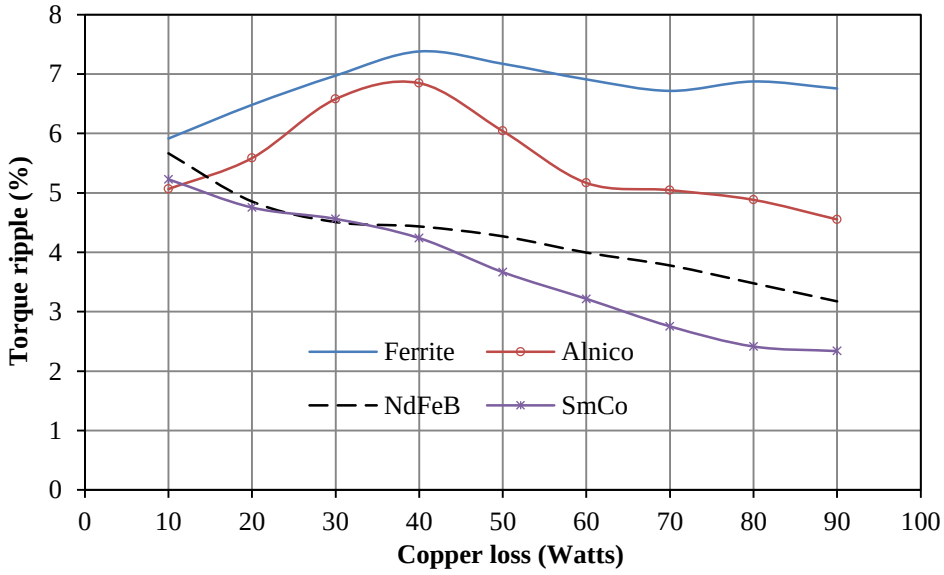

(b) Torque ripple versus copper loss

Figure 7: Comparison of total harmonic distortion and torque ripple

4.0. Conclusion

The impact of magnetic properties on the output performance of a dual stator permanent magnet machine is presented. A quantitative comparison of different magnet types is made. It is revealed that the coercive force and residual magnetic flux density of an electric machine would largely affect its output characteristics. Moreover, the machine type having neodymium magnet exhibit both the most promising torque profile and best saturation-withstand capability amongst all. The analyzed machine could be applied in low speed high torque uses, such as in-wheel machine application(s). Above all, electrical machine designers would obtain more insight on the need to select appropriate magnetic material for improved performance and for different application(s).

References

Wu, W; X. Zhu, L. Quan, Y. Hua and Q. Lu. 2018. Comparative study of IPM synchronous machines with different saliency ratios considering EVs operating conditions. Progress in Electromagnetics Research M, 71: 19–29.

Chen, J.T; Z.Q. Zhu and D. Howe. 2008. Stator and rotor pole combinations for multi-tooth flux-switching permanent-magnet brushless AC machines. IEEE Transactions on Magnetics, 44(12): 4659–4667.

Chen, Q; S. Eduku and W. Zhao. 2020. A new fault-tolerant switched flux machine with hybrid permanent magnets. CES Transactions on Electrical Machines and Systems, 4(2): 79–86.

Evans, D.J. and Zhu, Z.Q. 2015. Novel partitioned stator switched flux permanent magnet machines. IEEE Transactions on Magnetics, 51(1): 1–14.

Galioto, S.J; P.B. Reddy, A.M. EL-Refaie and J.P. Alexander. 2015. Effect of magnet types on performance of high-speed spoke interior-permanent-magnet machines designed for traction applications. IEEE Transactions on Industry Applications, 51(3): 2148–2160.

Ghorbanian, V; S. Hussain, S. Hamidizadeh, R. Chromik and D. Lowther 2018. The role of temperature-dependent material properties in optimizing the design of permanent magnet motors. IEEE Transactions on Magnetics, 54(3): 1–4.

Husain, T; I. Hasan, Y. Sozer, I. Husain and E. Muljadi. 2018. Design of a modular E-Core flux concentrating transverse flux machine. IEEE Transactions on Industry Applications, 54(3): 2115–2128.

Hwang, C; C. Chang, S. Hung and C. Liu. 2014. Design of high performance flux switching PM machines with concentrated windings. IEEE Transactions on Magnetics, 50(1): 1–4.

Liu, C; G. Lei, B. Ma, Y. Wang, Y. Guo and J. Zhu. 2017. Development of a new low-cost 3-D flux transverse flux FSPMM with soft magnetic composite cores and ferrite magnets. IEEE Transactions on Magnetics, 53(11): 1–5.

Maroufian, S.S. and Pillay, P. 2019. Design and analysis of a novel PM-Assisted synchronous reluctance machine topology with alnico magnets. IEEE Transactions on Industry Applications, 51(3): 4733–4742.

Paula, G.T; J.R.B.A. Monteiro, B.P. Alvarenga, T.E.P. Almeida, W.C.A. Pereira and M.P. Santana. (2018). On-load back EMF of PMSM using Maxwell stress tensor. IEEE Transactions on Magnetics, 54(7): 1–15.

Soleimani, J; A. Vahedi, A. Ejlali and M.B. Bafghi. 2014. Study on interior permanent magnet synchronous motors for hybrid electric vehicle traction drive application considering permanent magnet type and temperature. Turkish Journal of Electrical Engineering and Computer Sciences, 22(6): 1517–1527.

Wu, W; X. Zhu, L. Quan, Y. Du, Z. Xiang and X. Zhu. 2018. Design and analysis of a hybrid permanent magnet assisted synchronous reluctance motor considering magnetic saliency and PM usage. IEEE Transactions on Applied Superconductivity, 28(3): 1–6.

Xia, B; W. Fei, P. C. K. Luk and D. Wu. 2014. Design of a multi-layer interior ferrite permanent magnet synchronous machine for traction applications. Paper presented at the 7th IET International Conference on Power Electronics, Machines and Drives (PEMD 2014), Manchester, UK, 1–6.

Yu, C; S. Niu, S.L. Ho, W. Fu and L. Li. 2015. Hysteresis modeling in transient analysis of electric motors with AlNiCo magnets. IEEE Transactions on Magnetics, 51(3): 1–4.

Zhu, X; L. Wang, Y. Chen, L. Chen and L. Quan. 2015. A non-rare-earth doubly salient flux controllable motor capable of fault-tolerant control. IEEE Transactions on Magnetics, 51(11): 1–4.

Zhu, X; Y. Chen, Z. Xiang, L. Yang and L. Xu. 2016. Electromagnetic performance analysis of a new stator-partitioned flux memory machine capable of online flux control. IEEE Transactions on Magnetics, 52(7): 1–4.